Microelectronics Reliability 137 (2022) 114747

Contents lists available at ScienceDirect

Microelectronics Reliability

journal homepage: www.elsevier.com/locate/microrel

TID evaluation based on variabilities of space radiation and device failure dose in typical navigation satellite orbits

Jian-zhao Wang [a,b,*], Zhuo-xi Huo [a], Fang-fang Wang [c]

[a] Qian Xuesen Laboratory of Space Technology, China Academy of Space Technology, Beijing 100094, China
[b] Department of Astrophysical and Planetary Science, University of Colorado Boulder, CO 80309, USA
[c] Institute of Electronics, Chinese Academy of Sciences, Beijing 100190, China

ARTICLE INFO

Keywords:
Total ionizing dose
Radiation effect
Geosynchronous orbit
Medium earth orbit

ABSTRACT

Navigation satellites mainly operate in Medium Earth Orbit (MEO), Geostationary Earth Orbit (GEO), and Inclined Geosynchronous Satellite Orbit (IGSO). These orbits lie in or repeatedly cross the outer Van Allen belt of Earth. With large uncertainty, the radiation in these orbits mainly comes from electrons trapped in the outer radiation belt and solar energetic protons. The accurate design of the radiation shielding structure plays an important role in improving the efficiency of satellites. We introduce a method that incorporates the radiation variability in space and failure dose uncertainty of devices to evaluate the survival probability of devices caused by the Total Ionizing Dose (TID) effect. After fitting the failure dose data of operational amplifier TL084 by the Weibull distribution, we calculate the Confidence Levels (CLs) of all possible parameters of the distribution. Based on these parameters and the cumulative probability distribution of TID from space, we evaluate the effects of shielding thickness and mission duration on TL084's failure possibility at different CLs in MEO/GEO/IGSO. Furthermore, the required shielding thickness and the expected survival duration to ensure that TL084 could operate safely at specific CL are also investigated. By using this method, we could approach a balance among the device's ability, the shielding thickness, the expected duration of safe operation, and the confidence level of the design.

1. Introduction

The radiation environment in the outer Van Allen belt of Earth is very hash and dynamic [1]. The outer radiation belt is filled with relativistic electrons and these energetic particles pose risks for spacecraft that operate within it through harmful effects on the electronics and materials, including the Total Ionizing Dose (TID) effect [2], the internal charging effect [3], and the Single Event Effect (SEE) [4]. Many navigation satellites operate in the outer radiation belt. The US Global Positioning System (GPS) consists of more than 30 operational satellites in Medium Earth Orbit (MEO) with a 20,200 km altitude and the inclination is 55° [5]. The European Galileo navigation system operates at 23,222 km altitude with an inclination of 56° [6]. The Chinese Beidou navigation system includes 35 satellites in Geostationary Earth Orbit (GEO, 35,786 km × 0°), Inclined Geosynchronous Satellite Orbit (IGSO, 35,786 km × 55°), and MEO [7].

TID degradation of electronic devices caused by the radiation from energetic particles is a major cause of satellite operation anomalies. In GEO, the satellite locates near the outer edge of the outer Van Allen belt. The flux variation of energetic particles mainly comes from the solar eruption event [8] and the magnetic storm [9]. In MEO or IGSO, the satellite repeatedly crosses the outer radiation belt and the flux of energetic particles fluctuates a lot because of the large tilt angle of the orbit. In navigation satellite design, the TID design specification does not distinguish between different orbits. However, the spatial and temporal variations of radiation environment in MEO, GEO, and IGSO are very different. So it is necessary to examine the failure process of the electronic device in different orbits in detail.

In the TID hardness design, we should ensure that the device will not fail in orbit. So the failure doses of the device and the dose from the radiation environment should be known. However, the failure dose of devices from one lot is random in nature and obeys some probability distributions (e.g. normal, lognormal, or Weibull distribution) [10]. In addition, the radiation environment in the outer Van Allen belt is also very dynamic and variable. Historically, Radiation Design Margin (RDM) is also used to bind the uncertainties of the device's failure dose

* Corresponding author at: Qian Xuesen Laboratory of Space Technology, China Academy of Space Technology, Beijing 100094, China.
E-mail address: wangjz1989@126.com (J.-z. Wang).

https://doi.org/10.1016/j.microrel.2022.114747
Received 25 November 2021; Received in revised form 25 July 2022; Accepted 15 August 2022
Available online 24 August 2022

and radiation environment [11]. RDM is defined as the mean failure dose of the device divided by the mean radiation level expected from the environment. If RDM is properly selected, the device will be well operated even if some random or unexpected situations occur in orbit [12].

Benefitting from the rapid increase of space missions, a huge amount of in-situ data in the Van Allen belt are accumulated and the radiation environment models are much improved in recent years. Based on the probabilistic environment model, Xapsos et al. [13] introduced a new method that incorporated environmental variability to evaluate the failure probability of the device. Furthermore, Wang et al. [14] applied this method in Jupiter orbiting mission, in which TID is a major constraint in the mission design. Austin et al. [15] also utilized this concept in SEE evaluation. The probability of catastrophic failure from Single Event Burnout (SEB) for 1200 V Silicon Carbide (SiC) power Metal-Oxide-Semiconductor Field-Effect Transistors (MOSFETs) is evaluated. However, Xapsos et al. [13] only account for radiation environment uncertainty. Ladbury and Carstens [16] incorporated the confidence levels (CLs) of the device's failure dose distributions into the method from Xapsos et al. [13] and could obtain the failure probabilities of the device at different CLs.

The developments of the probabilistic environment models are the premises to use the method in Xapsos et al. [13] and Ladbury and Carstens [16]. In the outer Van Allen belt, the main radiation sources for TID are Solar Energetic Particles (SEPs) and particles trapped in Earth's magnetic field. Fortunately, many SEPs models were developed to output solar energetic particle fluence with different percentiles, including the King model [17], the JPL model [18], the Emission of Solar Proton (ESP) model [19], and the Moscow State University (MSU) model [20]. In recent years, new models of solar proton [21,22] and electron [23] were reported based on Virtual Timeline Method (VTM) to generate a timeline of events interspersed with waiting times. The fluences with CLs are obtained by repeating many iterations of VTM and ranking the results. However, before the release of the AP9/AE9 model [24], the trapped particle flux models in the Van Allen belt could only provide the mean result or had limited modes. The widely used AP8/AE8 [25] model could output proton/electron fluxes for solar maximum or minimum conditions. Other models are only applicable to specific orbits, e.g. the IGE-2006 model [26] in GEO and the MEO-v2 model [27] in MEO. The AP9/AE9 model could evaluate the dynamics of the trapped particle environment and provide probabilistic results in the whole region of the Van Allen belt. So combining probabilistic models for trapped and solar particles with the radiation test data of devices from one lot, we could quantitative evaluate the performance of devices in different orbits.

2. Method and data

From Xapsos et al. [13], the failure probability P_{fail} of the irradiated devices is as follows:

$$P_{fail} = \int [1 - H(x)] \cdot g(x) \mathrm{d}x \tag{1}$$

where x is the total dose. $H(x)$ is the Cumulative Distribution Function (CDF) of radiation dose from space during the mission period. So $[1 - H(x)]$ is the probability that the mission dose exceeds x. $g(x)$ is the Probability Distribution Function (PDF) of the devices' failure doses and is the possibility that the device fails between doses x and $x + \mathrm{d}x$. So after integration, we could obtain the failure probability of the device due to the TID effect within the mission period. Fig. 1 illustrates the three possible relations between $[1 - H(x)]$ and $g(x)$. In panel (a), if the mean mission dose is much smaller than the mean device failure dose, $[1 - H(x)] \cdot g(x) \approx 0$ when x takes any value. So $P_{fail} \approx 0$ after the integration. On the contrary, if the mission dose is much larger than the device failure dose, as panel (c) shows, $[1 - H(x)] \cdot g(x) \approx g(x)$ when $x < x_1$ and $[1 - H(x)] \cdot g(x) \approx 0$ when $x > x_1$. So $P_{fail} \approx 1$ after the integration. In these two situations, the uncertainties of device failure dose and mission dose have little effect on P_{fail}. In panel (b), if these two distributions overlap, P_{fail} is within $0 \sim 1$ after integration and is sensitive to the uncertainties of device failure dose and mission dose.

2.1. Failure doses of devices

The failure doses of devices are always obtained by radiation test of $^{60}\mathrm{Co} - \gamma$ facilities in the laboratory. The failure dose distributions vary with different types or lots of devices. In this study, we select the quad operational amplifier TL084, which is widely used in space for data acquisition. In the test, eight devices from one single lot are irradiated by ^{60}Co source at a rate of 50 rad(Si)/s with a maximum dose of 100 krad (Si).

In the radiation test, the supply voltage on TL084 is 15 V. According to ASTM-F1892 Standard Guide for Ionizing Radiation (Total Dose) Effects Testing of Semiconductor Devices, if known, the bias applied to the test devices should be selected to produce the worst-case damage. However, the determination of the worst-case bias is often a complex process. In addition, according to QJ 10004-2008, if the worst-case bias condition is unknown, the test could also be performed under the working voltage under the premise that the results could only be used in this bias condition. So the bias voltage in the test is set as 2 V.

An illustration of the test setup is shown in Fig. 2. In the radiation room, the radiation source consists of many ^{60}Co rods, which are arranged as a cylindrical structure. So the inhomogeneity of radiation is less than 10 % in the test. All eight devices are tested under the same biased voltage. The test benches have different distances from the ^{60}Co source, so the dose rates are different. Dosimeters are also placed near these test benches to measure the actual dose. In the test room, the test computer and DC power are connected to the test bench through cable and sample the data in real-time.

After radiation, almost all electrical parameters of the operational amplifier should deteriorate to varying degrees. Among these

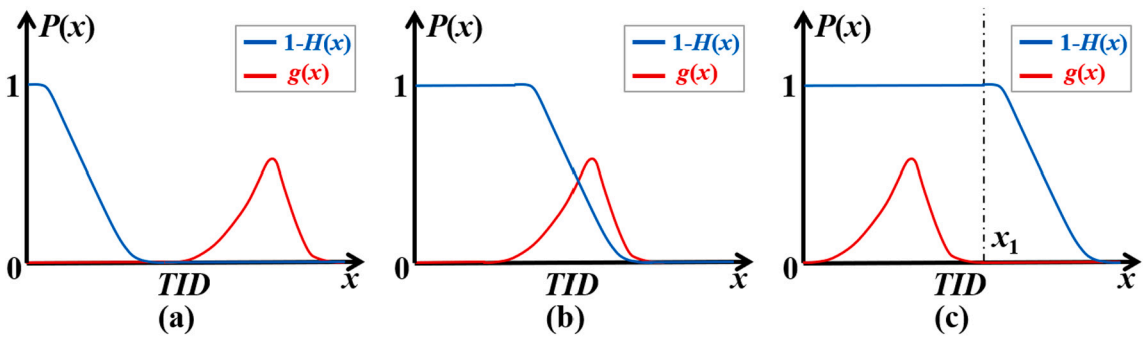

Fig. 1. Illustration of the device failure possibility evaluation method in Xapsos et al. [13].

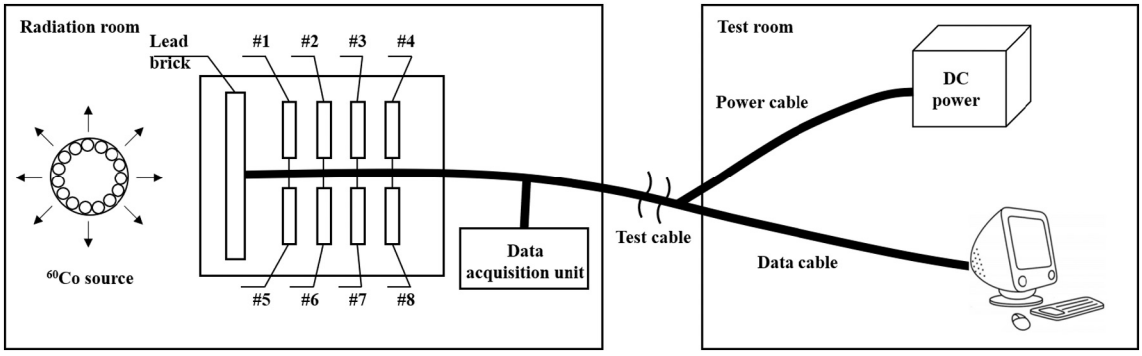

Fig. 2. Illustration of the test setup.

parameters, the change of the positive bias current is the most dramatic and the bias current directly reflects the value of the amplification factor of a transistor (β). The rapid increase of the bias current will lead to the attenuation of β. So we measured the positive bias currents at different cumulative doses and the results are shown in Fig. 3. We assume that the parametric failure occurs at the dose when the bias current increases 1000 times to exceed $10^{-3}\mu$A, as the dotted line shows in Fig. 3. Then the failure doses of these eight devices are calculated by linear interpolation and the results are shown in Table 1.

To obtain $g(x)$ in Eq. (1), we should use some distributions to fit the failure dose data of these devices. Gaussian, lognormal, and Weibull distributions are usually chosen. We use the coefficient of determination R^2 to define if the distribution is good enough and R^2 is defined as:

$$\begin{cases} R^2 = 1 - \mathrm{SSE}/\mathrm{SST} \\ \mathrm{SSE} = \sum (y - y^*)^2 \\ \mathrm{SST} = \sum (y - \bar{y})^2 \end{cases} \tag{2}$$

where SSE is the sum of squares due to error, SST is the total sum of squares, y is the measured value, $\bar{y}$ is the mean value of y, and y^* is the predicted value by the fitting algorithm. The result is shown in Table 2 and the Weibull fitting is the best among these three distributions.

The Weibull distribution is:

$$f(x,a,b) = (b/a^b)x^{b-1}exp\left(-(x/a)^b\right) \tag{3}$$

where x is the failure dose of TL084. a and b are the two parameters of the Weibull distribution. However, these two parameters have

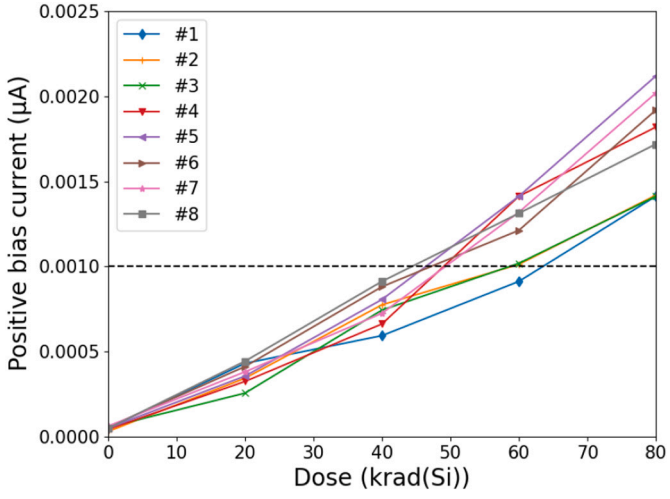

Fig. 3. Positive bias currents as a function of total dose for eight TL084 quad operational amplifiers.

Table 1
Failure doses of TL084 when positive bias currents exceed $1 \times 10^{-3}\mu$A.

Part	#1	#2	#3	#4	#5	#6	#7	#8
Failure dose (krad(Si))	65.0	61.0	61.1	51.0	48.0	49.1	51.3	45.8

Table 2
Determination coefficient of TL084 failure dose fitting.

Fitting type	Gaussian	lognormal	Weibull
R^2	0.805	0.819	0.863

uncertainty because the number of irradiated samples is limited and we are not sure about the confidence of each pair of parameters. Following the method in Ladbury and Carstens [16], the likelihood for a data set $\{x_i\}$ is:

$$L(\{x_i\}) = \prod_i f(x_i, a, b) \tag{4}$$

The values of a and b that maximize the likelihood are called the Maximum Likelihood Estimators (MLEs) for the distribution and give the best fit to the data in a maximum likelihood sense. In addition, the logarithm of the likelihood ratio relative to the maximum likelihood as parameter values move away from the MLEs tends to be distributed as the χ^2 distribution:

$$ln\left(\frac{L(\{x_i\}, \mathrm{CL})}{L(\{x_i\}, Max)}\right) = -0.5 \times isf(1 - \mathrm{CL}, \mathrm{DOF}) \tag{5}$$

where $L(\{x_i\}, \mathrm{CL})$ is the likelihood at the CL confidence level. $L(\{x_i\}, \mathrm{Max})$ is the maximum likelihood. *isf* is the inverse survival function of the χ^2 distribution. DOF is the degree of freedom of the χ^2 distribution and equals the number of parameters for the distribution (i.e. DOF = 2 in the Weibull distribution). Fig. 4 shows the logarithms of the likelihood ratios for various Weibull fit parameters, along with the maximum and 75 %, 80 %, 85 %, 90 %, 95 %, and 99 % confidence contours. In this way, we could evaluate the confidence of one pair of parameters in the Weibull distribution. The MLEs are $a = 57.1$ and $b = 8.6$ for the Weibull distribution of TL084 failure dose. The increase in CL leads to an expansion of the 'circle' designated by the contour. This means that if we expand the selection range of a and b, we are more confident that the 'real' parameters of failure dose distribution are within the selected range.

Define that $G(x)$ is the Cumulative Distribution Function (CDF) of $g(x)$. After taking all values of a and b within 99 % CL, we could obtain all possible Weibull distributions of device failure dose. The cumulative failure probabilities (i.e. $G(x)$) of all distributions are shown in Fig. 5 and distributions within different CL intervals are designated by different colors. The black solid line represents the distribution of maximum

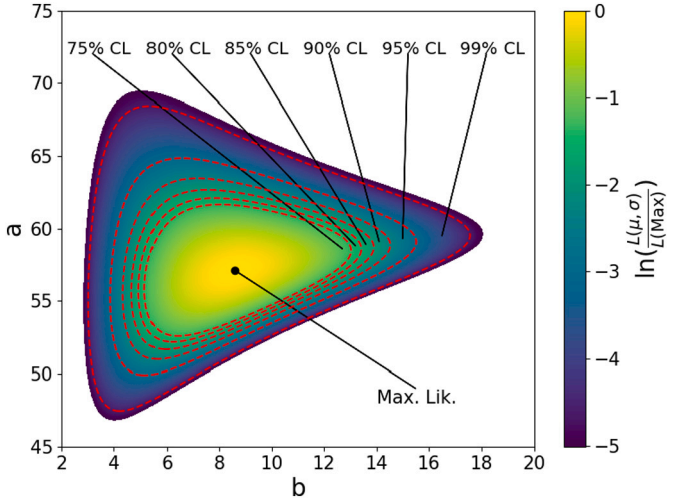

Fig. 4. Contour of the logarithms of the likelihood ratios relative to the maximum likelihood of TL084 failure doses for the Weibull distribution.

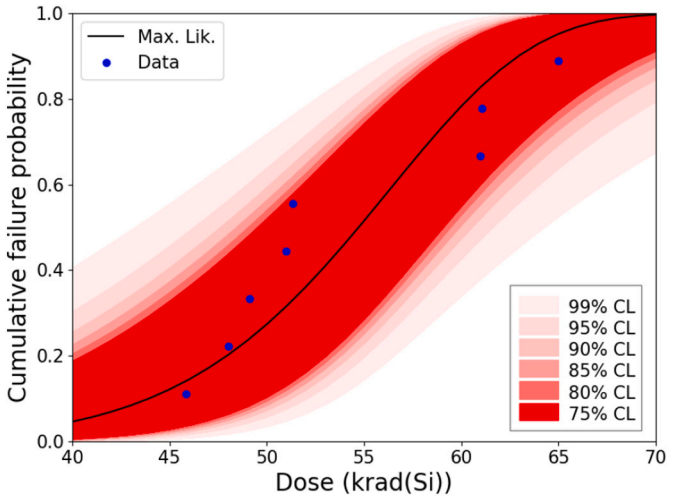

Fig. 5. Weibull fit of TL084 cumulative failure probability.

likelihood. Similar to Fig. 4, the increase in CL leads to an expansion of the area designated by the boundary. In this way, we could evaluate the confidence of failure possibilities at different dose values. Then it is easy to get $g(x)$ within different CLs after differential calculation of $G(x)$.

2.2. Radiation environments

In the navigation satellite orbits, the radiation that causes TID is mainly from trapped energetic particles in the Van Allen belt and solar proton. We use the AP9/AE9 model to calculate the trapped proton and electron fluences in MEO (20,200 km × 55°), GEO (35,786 km × 0°), and IGSO (35,786 km × 55°). This model is developed based on in-situ data from various orbits and could output energetic particle flux at different confidence levels. AP9/AE9 provides three modes: the mean or percentile, the perturbed mean, and the Monte Carlo modes with random perturbation. We use the perturbed mean mode to repeatedly calculate the energetic particle flux along the orbit 99 times. Then the resulting fluence is separately ranked by percentile according to $m/(N+1)$, where m is the ordered rank and $N = 99$ is the number of calculations. The mean electron flux in MEO/GEO/IGSO is shown in Fig. 6. The solid lines show the variations of the mean flux along the orbit and the dotted lines show the averaged value of the flux. In general, due to the inclinations of the orbits, spacecraft in MEO and IGSO traverse in and out

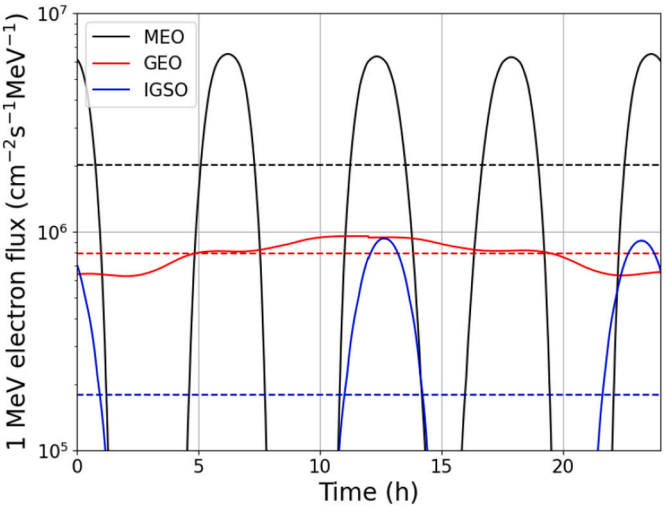

Fig. 6. The mean 1 MeV electron flux in MEO/GEO/IGSO.

of the outer Van Allen belt repeatedly. The fluxes in MEO and IGSO fluctuate a lot with periods of 12-hour and 24-hour, respectively. For GEO, the variation range of the electron flux along the orbit is small. The intersection of MEO and the magnetic equatorial plane is located near the center of the outer Van Allen radiation belt. So the averaged flux in MEO is greater than that in GEO and IGSO. In addition, because of the inclination of IGSO, the averaged flux in GEO is greater than that in IGSO.

Furthermore, we use the newly developed SAPPHIRE model [22] to calculate the solar proton fluence. This model is based on over 40 years of cleaned and processed in-situ data and uses the virtual timeline method to generate virtual events in the mission period. The spectra of solar protons in Earth's vicinity at different confidence levels are shown in Fig. 7. In general, the fluence from the Van Allen belt is about 3–4 magnitude higher than that from the solar proton.

3. Results

In order to get $H(x)$ in Eq. (1), the mission dose should be described probabilistically. Considering the fluences from both solar proton and the Van Allen belt, we compute the dose-depth curves in MEO/GEO/IGSO with different percentiles after aluminum (Al) shielding using the solid sphere shielding model of the SHIELDOSE2 code. For 2 mm Al shielding, the corresponding CDFs of one-year mission TIDs (i.e. $H(x)$)

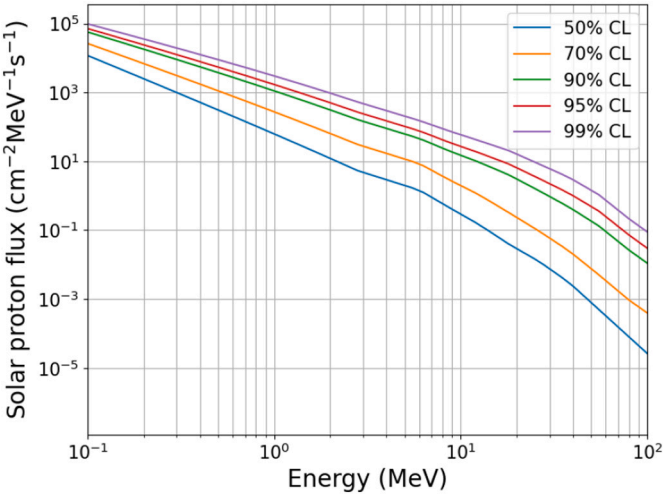

Fig. 7. Differential spectra of solar proton at different confidence levels.

are shown in Fig. 8. Relative to the value of 50 % percentile, the mission TIDs are anti-symmetrically distributed. This implies that $h(x)$ (i.e. the PDF of mission TID) conforms to the lognormal distribution. In the high percentile region, the increase of TID is respectively greater than the increase in percentile. Define $\delta D = (D_{99} - D_1)/D_{50}$ is the variability of TID, where D_{99}, D_{50}, and D_1 are TIDs at 99 %, 50 %, and 1 % percentiles, respectively. The radiations in IGSO ($\delta D = 1.37$) and GEO ($\delta D = 1.39$) are more variable than that in MEO ($\delta D = 0.57$), respectively.

Based on $g(x)$ at different CLs and $H(x)$ at different shielding thicknesses, we calculate the failure possibility of TL084 in one year mission after different shieldings, as shown in Fig. 9. The boundaries of different CLs are also shown in the figure. The results combine the variabilities of radiation environment and device's failure dose and show how the device's survival possibility changes with shielding thickness. For example, in GEO, if the shielding thickness is smaller than 1.8 mm, the radiation from space is much greater than the device's failure dose and $P_{fail} \approx 1$. On the contrary, if the thickness is greater than 3.3 mm, the radiation in GEO is much less than the radiation resistance of the device and $P_{fail} \approx 0$. If the thickness is between 1.8 mm and 3.3 mm, the uncertainties of environmental radiation and the device's failure dose overlap, so P_{fail} is within 0 and 1. In general, for the same shielding, the failure probabilities of TL084 in MEO, GEO, and IGSO decrease in turn. The failure possibility decreases rapidly with the increase of shielding thickness. If the maximum acceptable failure probability of TL084 is 0.5, the required shielding thickness with maximum likelihood in MEO/GEO/IGSO is 3.3 mm/2.5 mm/1.3 mm.

In the design, the shielding thickness with the best cost-effectiveness ratio could be selected according to this method, i.e. the minimum shielding to achieve a respectively high survival probability. The result in MEO is shown in Fig. 10 and other examples in GEO and IGSO are provided in the Appendix A section. Define the survival probability P_s equals 1 minus the failure probability P_{fail}, different curves in Fig. 10 correspond to different criteria. If the survival criterion of TL084 is $P_s \geq$ 50%, 3.4 mm Al shielding is needed at 95 % CL. Below 95 % CL, the required shielding thickness increases slowly with CL. Therefore it is not necessary to select a CL smaller than 95 % in the design. However, above 95 % CL, the additional shielding required to increase CL is costly and the tradeoffs need to be considered in the design. In addition, an increase in P_s as the survival criterion also results in an obvious increase in the required shielding thickness. At 95 % CL, if the survival probability of TL084 needs to be increased from 50 % to 99 %, the required Al shielding thickness should be increased from 3.4 mm to 4.0 mm. In summary, we could approach a balance among the device's ability of radiation resistance, the shielding thickness, and the confidence level of the design by using this method.

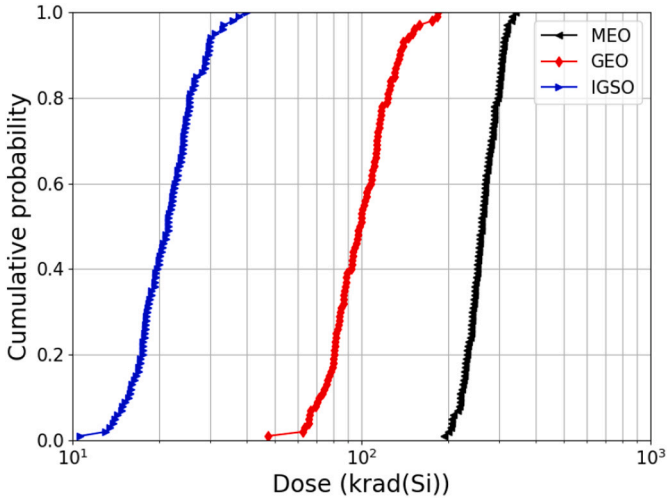

Fig. 8. Cumulative probability distribution of total dose from the one-year mission after 2 mm aluminum shielding in MEO/GEO/IGSO.

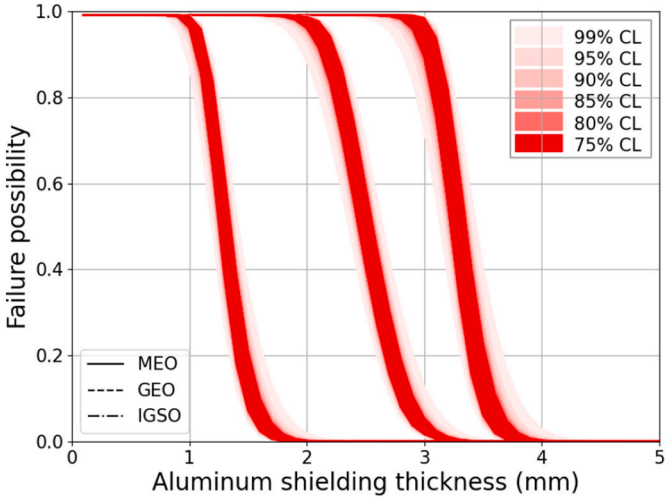

Fig. 9. Failure probability of TL084 versus shielding thickness for the one-year mission in MEO/GEO/IGSO.

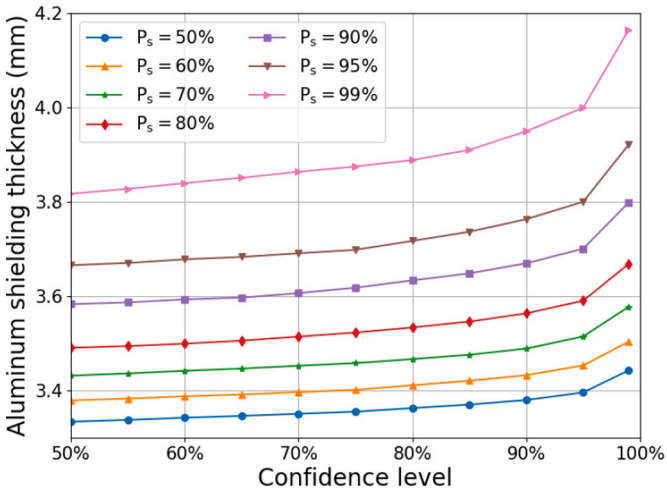

Fig. 10. The required aluminum shielding thickness to achieve the corresponding survival probability of TL084 at different confidence levels for the one-year mission in MEO.

We also investigate the survival possibility of TL084 versus mission duration in MEO, GEO, and IGSO after 4 mm Al shielding, as shown in Fig. 11. Similarly, the boundaries of different CLs are also shown in the figure. In general, with the increase in mission duration, the survival probability P_s of TL084 decreases rapidly and reaches complete failure (i.e. $P_s = 0$) slowly. As suggested in Guenther [28], the survival probability decays exponentially with mission duration: $P_s = \exp(-a \cdot t)$, where a is the failure rate. Above $P_s \geq 0.5$, the failure rate of TL084 increases with mission duration. On the contrary, the failure rate of TL084 decreases with mission duration if $P_s \leq 0.5$. Taking $P_s = 0.5$ as the criterion, the durations of the normal operation of TL084 with maximum likelihood in MEO, GEO, and IGSO are 2.2 years, 6.0 years, and 28.2 years, respectively.

After determining the shielding thickness, we can deduce the expected durations that TL084 could operate safely at different CLs. The result in MEO after 4 mm Al shielding is shown in Fig. 12. Other results in GEO and IGSO are provided in the Appendix A section. If the survival criterion of TL084 is $P_s \geq$ 50%, the safe operation duration of TL084 is 1.94 years at 95 % CL. Below 95 % CL, the duration decreases slowly with CL and it is not necessary to select a CL smaller than 95 % in the

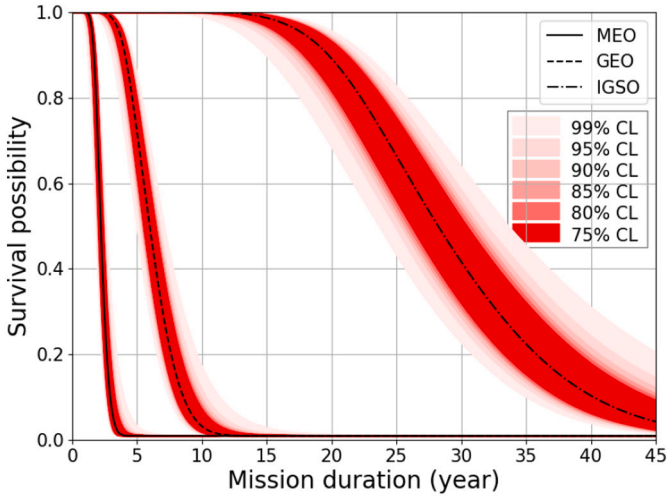

Fig. 11. Survival probability of TL084 versus mission duration in MEO/GEO/IGSO after 4 mm aluminum shielding.

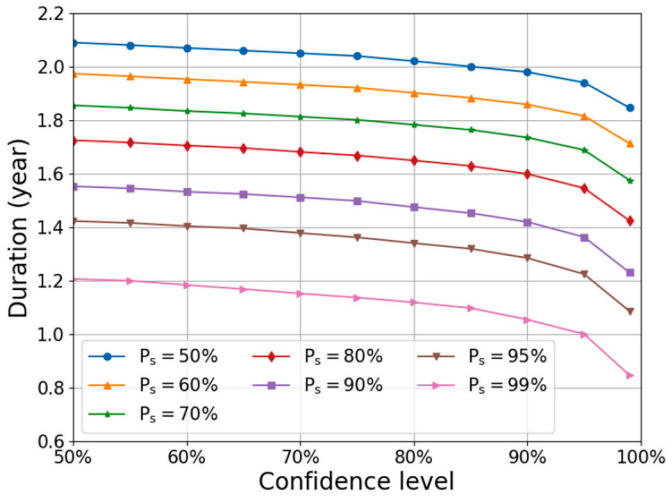

Fig. 12. The survival duration of TL084 at different confidence levels under different criteria represented by survival probability in MEO after 4 mm aluminum shielding.

design. However, above 95 % CL, the expected duration decreases rapidly with CL. In addition, an increase in P_s as the survival criterion also results in an obvious decrease in the expected duration that TL084 could operate safely. At 95 % CL, if the criterion is raised from $P_s = 50\%$ to $P_s = 99\%$, the expected duration decreases from 1.94 year to 1.0 year. In this way, we could approach a balance among the device's ability, the expected duration of safe operation, and the confidence level of the design.

4. Summary

In MEO, GEO, or IGSO, the satellite lies in or repeatedly crosses the outer Van Allen belt of Earth. The energetic proton and electron environments in these orbits are very hash with high uncertainty. Therefore the protection of radiation from energetic particles is the key factor to ensure the safe operation of navigation satellites. On the other hand, the properties of performance degradation of devices in radiation are different and follow certain distributions. In this study, we develop a method to evaluate the survival possibility (P_s) of the device caused by the Total Ionizing Dose (TID) effect after shielding layers. This method incorporates the variabilities of space radiation and device failure dose to calculate the performance degradation process of the device quantitatively.

Eight devices from one lot are irradiated by the $^{60}Co - \gamma$ facility and the two-parameter Weibull distribution is used to fit the failure dose data. The confidence levels (CLs) of different parameters are calculated according to the likelihood statistical model. Then we get the CLs of the corresponding failure dose distributions of TL084. Furthermore, we use the AP9/AE9 model to calculate the energetic electron flux at different percentiles from the Van Allen belt in MEO/GEO/IGSO. The solar proton flux at different percentiles is also calculated by the SAPPHIRE model. Then the cumulative probability distributions of TID in MEO/GEO/IGSO are obtained by combining the contributions from energetic electrons and solar protons. By incorporating the failure dose of TL084 and TID from space, the survival possibilities of TL084 in different situations are investigated.

We first study the failure probabilities of TL084 after different shielding conditions. In the one-year mission, 3.3 mm/2.5 mm/1.3 mm aluminum shielding is needed to guarantee the survival probability of TL084 is greater than 0.5 in MEO/GEO/IGSO. Then the required shielding thickness to achieve the corresponding survival probability at specific CL is investigated. At 95 % CL, in order to increase the survival probability of TL084 from 50 % to 99 % in MEO, the required shielding needs to be increased from 3.4 mm to 4.0 mm. Furthermore, we study the performance of TL084 with mission duration. If $P_s = 0.5$ is selected as the criterion, the lifetime of TL084 is 2.2 years/6.0 years/28.2 years in MEO/GEO/IGSO. Then the expected lifetime at specific criterion and CL is investigated. At 95 % CL, if the criterion is raised from $P_s = 50\%$ to $P_s = 99\%$, the expected lifetime of TL084 in MEO decreases from 1.94 years to 1.0 years. In conclusion, we could realize the optimal design of the shielding structure using this method.

5. Discussion

According to ASTM-F1892 Standard Guide for Ionizing Radiation (Total Dose) Effects Testing of Semiconductor Devices, there should be at least 5 samples for each set of test conditions. In principle, more samples could produce more accurate information about the failure probability distribution of the device. However, the number of samples is also limited by the radiation test conditions. The number 8 is a result of a compromise between fitting quality and test conditions.

We illustrate how the numbers of samples influence the results, as shown in the Appendix B section. Panel (a) is the same as that in Fig. 5. In Panel (b), we add two artificial data points (represented by the yellow solid circles) that are completely consistent with the Weibull distribution. As a result, compared with Panel (a), the area between 75 % confidence level intervals in Panel (b) decreases, due to the addition of the artificial data points. That means more samples could help constrain the distribution of the device's failure dose.

In the radiation test, all devices are from the same lot. They are made of the same material and the same process. If we use the devices from different lots, the degeneration behavior after radiation should be different. Because the materials (i.e. silicon wafer) and process operations involved in different lots of devices may change. So the distribution of failure dose should be more complicated than what we got. Furthermore, the difference should be larger if the devices are from different vendors.

Enhanced Low Dose Rate Sensitivity (ELDRS) effect is important in bipolar linear transistors. It means that with the same cumulative total dose, the damage under the low dose rate is greater than that under the high dose rate, respectively. In principle, the device with the ELDRS effect should be tested under the low dose rate (0.01–0.1 rad(Si)/s) condition. However, the failure dose of TL084 is about several tens of krad(Si), so the radiation test under the low dose rate condition could last for more than 10 days and it is not acceptable.

The method in this paper is general because the variabilities of space radiation and device failure dose are universal. However, the

effectiveness of this method also depends on many factors. First, the failure possibility derived from this method is sensitive if the distributions of device failure dose and mission dose overlap. Otherwise, the advantages of this method cannot be well reflected. Second, this method is valid only when the data of the device's failure dose reflects good statistics. If the data is highly discrete and could not be well fitted by some distributions, the failure probability deduced from this method is not credible.

Evaluation of failure possibility is complex and difficult. At different levels (i.e. component, device, circuit, instrument, subsystem, spacecraft), the evaluation method varies a lot. In addition, according to different fabrication processes, the degeneration of devices also varies a lot. So this paper only gives an example of how to treat this complex problem at the device level and how to evaluate the failure dose quantitatively and statistically. In addition, this paper focuses on the statistics, other than the device itself.

CRediT authorship contribution statement

Under supervision by Zhuo-xi Huo, Jian-zhao Wang performed modeling, data analysis, visualizing, and writing. Fang-fang Wang performed reviewing and editing. All authors read and contributed to the manuscript.

Declaration of competing interest

The authors declare that they have no known competing financial interests or personal relationships that could have appeared to influence the work reported in this paper.

Data availability

Data will be made available on request.

Acknowledgments

The authors would like to thank the Air Force Research Laboratory for providing the AP9/AE9 model

Appendix A. The supplementary results in GEO and IGSO

The required shielding to achieve a survival probability at different confidence levels in GEO and IGSO are shown in Fig. A.13 and Fig. A.14, respectively. The expected duration of TL084 at different confidence levels in GEO and IGSO are shown in Fig. A.15 and Fig. A.16, respectively.

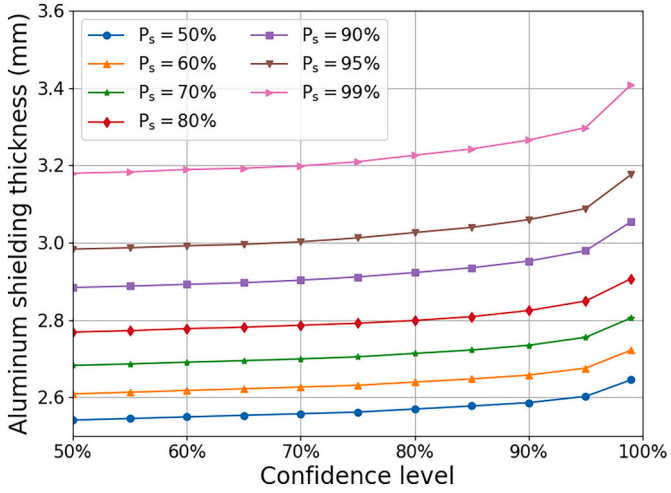

Fig. A.13. The required aluminum shielding thickness to achieve the corresponding survival probability of TL084 at different confidence levels for the one-year mission in GEO.

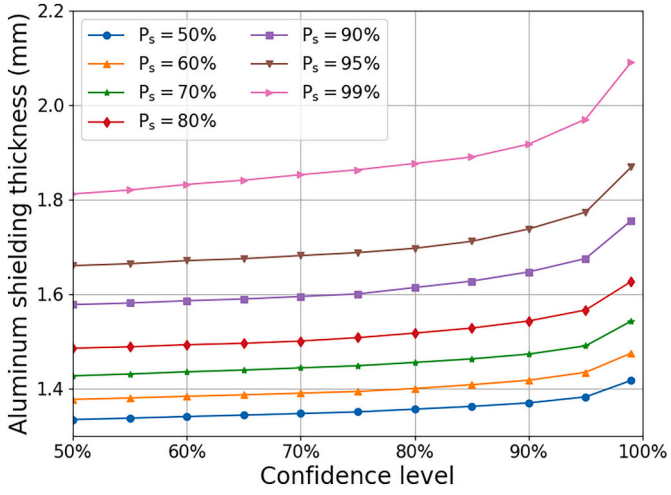

Fig. A.14. The required aluminum shielding thickness to achieve the corresponding survival probability of TL084 at different confidence levels for the one-year mission in IGSO.

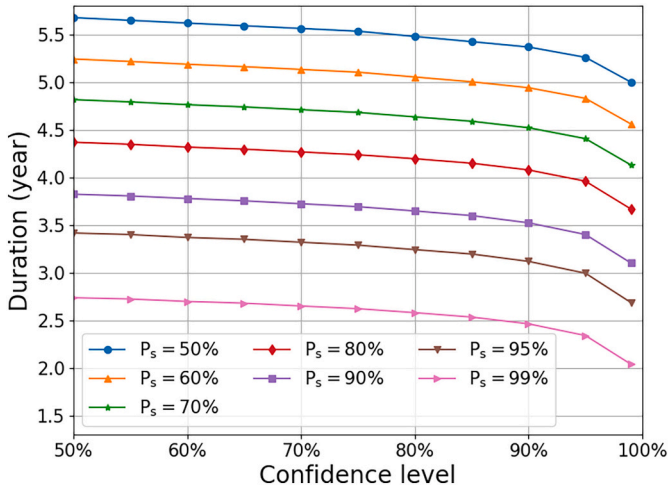

Fig. A.15. The survival duration of TL084 at different confidence levels under different criteria represented by survival probability in GEO after 4 mm aluminum shielding.

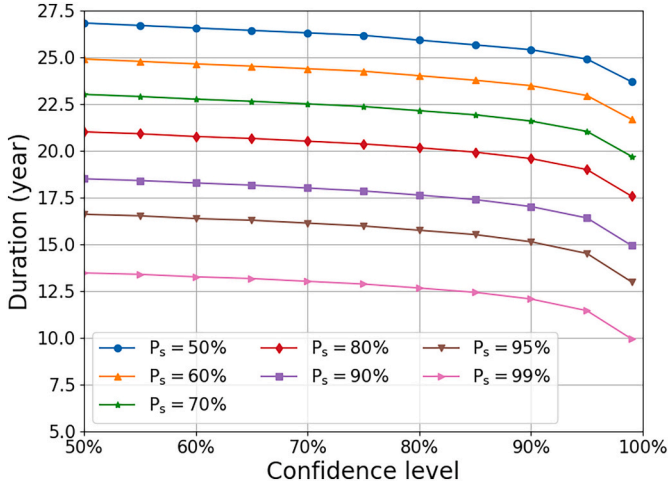

Fig. A.16. The survival duration of TL084 at different confidence levels under different criteria represented by survival probability in IGSO after 4 mm aluminum shielding.

Appendix B. The example of how the sample number influences the distribution fitting results

Fig. 17 shows how the sample number affect the distribution fitting by using some artificial data that are consistent with the Weibull distribution.

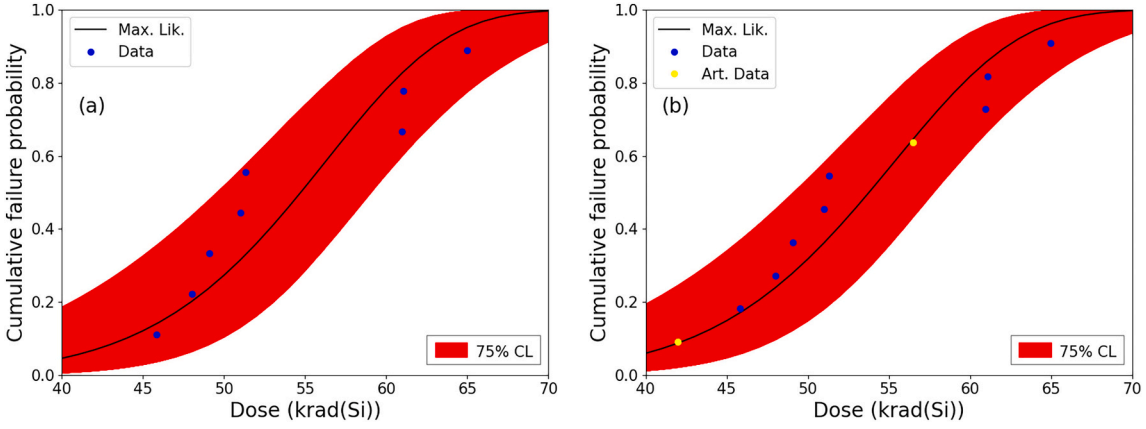

Fig. A.17. Weibull fit of TL084 cumulative failure probability (a) without and (b) with artificial data.

References

[1] J. Wang, Y. Hu, D. Yu, et al., Electron environment characteristics and internal charging evaluation for MEO satellite, IEEE Trans. Plasma Sci. 65 (8) (2018) 1685–1693, https://doi.org/10.1109/TNS.2018.2792049.

[2] Y. Chen, M.R. Carver, S.K. Morley, Determining ionizing doses in medium earth orbits using long-term GPS particle measurements, in: 2021 IEEE Aerospace Conference, Big Sky, MT, USA, 2021, https://doi.org/10.1109/AERO50100.2021.9438516.

[3] J. Wang, Y. Hu, D. Yu, et al., Internal charging characteristics in typical navigation satellite orbits, IEEE Trans. Plasma Sci. 46 (4) (2018) 1010–1017, https://doi.org/10.1109/TPS.2018.2811864.

[4] D.C. Wilkinson, M.A. Shea, D.F. Smart, A case history of solar and galactic space weather effects on the geosynchronous communications satellite TDRS-1, Adv. Space Res. 26 (1) (2000) 27–30, https://doi.org/10.1016/S0273-1177(99)01022-4.

[5] S.K. Morley, J.P. Sullivan, M.R. Carver, et al., Energetic particle data from the global positioning system constellation, Space Weather 15 (2017) 283–289, https://doi.org/10.1002/2017SW001604.

[6] C.C. Chao, R.A. Gick, Long-term evolution of navigation satellite orbits: GPS/GLONASS/GALILEO, Adv. Space Res. 34 (5) (2004) 1221–1226, https://doi.org/10.1016/j.asr.2003.01.021.

[7] F.P. Sun, S. Liu, X. Zhu, et al., Research and progress of beidou satellite navigation system, Sci. China Inf. Sci. 55 (12) (2012) 2899–2907, https://doi.org/10.1007/s11432-012-4724-2.

[8] R. Kataoka, Y. Miyoshi, Average profiles of the solar wind and outer radiation belt during the extreme flux enhancement of relativistic electrons at geosynchronous orbit, Ann. Geophys. 26 (2008) 1335–1339, https://doi.org/10.5194/angeo-26-1335-2008.

[9] M.F. Bakhareva, L.V. Tverskaya, K.G. Orlova, Specific features of the relativistic electron flux dynamics during the recovery phase of a magnetic storm on April 6, 2000, Geomagn. Aeron. 51 (3) (2011) 303–308, https://doi.org/10.1134/s0016793211030029.

[10] R. Ladbury, J.L. Gorelick, Statistical methods for large flight lots and ultra-high reliability applications, IEEE Trans. Nucl. Sci. 52 (6) (2005) 2630–2637, https://doi.org/10.1109/TNS.2005.861080.

[11] C. Poivey, Radiation hardness assurance for space system, in: IEEE Nuclear and Space Radiation Effects Conference, Phoenix, AZ, USA, 2002, https://doi.org/10.1109/AERO50100.2021.9438516.

[12] R. Ladbury, J.L. Gorelick, S.S. McClure, Statistical model selection for TID hardness assurance, IEEE Trans. Nucl. Sci. 56 (6) (2009) 3354–3360, https://doi.org/10.1109/TNS.2009.2033691.

[13] M.A. Xapsos, C. Stauffer, A. Phan, et al., Inclusion of radiation environment variability in total dose hardness assurance methodology, IEEE Trans. Plasma Sci. 64 (1) (2017) 325–331, https://doi.org/10.1109/TNS.2016.2607021.

[14] J. Wang, Q. Zhang, Y. Zheng, et al., TID and internal charging evaluation for Jupiter orbiting mission, IEEE Trans. Plasma Sci. 66 (2) (2019) 557–566, https://doi.org/10.1109/TNS.2018.2890660.

[15] R.A. Austin, B.D. Sierawski, R.A. Reed, et al., Inclusion of radiation environment variability for reliability estimates for SiC power MOSFETs, IEEE Trans. Nucl. Sci. 67 (1) (2020) 353–357, https://doi.org/10.1109/TNS.2021.3055694.

[16] R. Ladbury, T. Carstens, Development of TID hardness assurance methodologies to capitalize on statistical radiation environment models, IEEE Trans. Nucl. Sci. 68 (8) (2021) 1736–1745, https://doi.org/10.1109/TNS.2019.2957979.

[17] J.H. King, Solar proton fluences for 1977–1983 space mission, J. Spacec. Roc. 11 (6) (1974) 401–409, https://doi.org/10.2514/3.62088.

[18] J. Feynman, G. Spitale, J. Wang, et al., Interplanetary proton fluence model: JPL 1991, J. Geophys. Res. 98 (A8) (1993) 13281–13294, https://doi.org/10.1029/92JA02670.

[19] M.A. Xapsos, G.P. Summers, J.L. Barth, et al., Probability model for cumulative solar proton event fluences, IEEE Trans. Nucl. Sci. 47 (3) (2000) 22–26, https://doi.org/10.1109/23.856469.

[20] R.A. Nymmik, Probabilistic model for fluences and peak fluxes of solar energetic particles, Radiat. Meas. 30 (3) (1999) 287–296, https://doi.org/10.1016/S1350-4487(99)00065-7.

[21] P.T. Jiggens, S.B. Gabriel, D. Heynderickx, et al., ESA SEPEM project: peak flux and fluence model, IEEE Trans. Nucl. Sci. 59 (4) (2012) 1066–1077, https://doi.org/10.1109/TNS.2012.2198242.

[22] P. Jiggens, D. Heynderickx, I. Sandberg, Updated model of the solar energetic proton environment in space, J. Space Weather Space Climate 8 (2018), A31, https://doi.org/10.1051/swsc/2018010.

[23] J. Wang, Y. Wang, S.W. Dai, et al., A solar electron event model in near-earth space, Adv. Space Res. 64 (2019) 1825–1837, https://doi.org/10.1016/j.asr.2019.07.039.

[24] G.P. Ginet, T.P. O'Brien, S.L. Huston, et al., The AE9, AP9 and SPM: new models for specifying the trapped energetic particle and space plasma environment, Space Sci. Rev. 179 (1–4) (2013) 579–615, https://doi.org/10.1007/s11214-013-9964-y.

[25] C.E. Jordan, NASA Radiation Belt Models AP-8 and AE-8, RADEX, Inc, Bedford, MA. USA, 1989.

[26] A. Sicard-Piet, S. Bourdarie, D. Boscher, A new international geostationary electron model: IGE-2006, from 1 keV to 5.2 MeV, Space Weather 6 (2008), S07003, https://doi.org/10.1029/2007SW000368.

[27] A. Sicard-Piet, S. Bourdarie, D. Boscher, Solar cycle electron radiation environment at GNSS like altitude, in: 57th Int. Astron. Congr., Valencia, Spain, 2006, https://doi.org/10.2514/6.IAC-06-D5.2.04.

[28] C.F. Guenther, A method to quantitatively justify and relate shielding requirements and design margins to hardware requirements, in: IEEE 9th Digital Avionics System Conference, Virginia, USA, 1990, https://doi.org/10.1109/DASC.1990.111326.